13th World Conference on Earthquake Engineering
Vancouver, B.C., Canada
August 1-6, 2004
Paper No. 0301

TESTING AND MODELING FOR CYCLIC JOINT SHEAR DEFORMATIONS IN RC BEAM-COLUMN CONNECTIONS

Myoungsu SHIN[1] and James M. LAFAVE[2]

SUMMARY

In seismic analysis of moment-resisting frames, beam-column connections are often modeled with rigid joint zones. However, it has been demonstrated that, in ductile reinforced concrete (RC) moment-resisting frames designed based on current codes (to say nothing of older non-ductile frames), the joint zones are in fact not rigid, but rather undergo significant shear deformations that contribute greatly to global drift. The primary objective of this paper is to propose a rational method of estimating the nonlinear hysteretic joint shear behavior of RC beam-column connections and of incorporating this behavior into frame analysis. The authors tested four RC edge beam-column-slab connection subassemblies subjected to earthquake-type lateral loading; hysteretic joint shear behavior is investigated based on these tests and other laboratory tests reported in the literature. An analytical scheme employing the modified compression field theory (MCFT) is developed to approximate joint shear stress vs. joint shear strain response. A connection model capable of explicitly considering hysteretic joint shear behavior is then formulated for nonlinear structural analysis. The connection model is able to well represent the experimental hysteretic joint shear behavior and overall load-displacement response of the connection subassemblies.

[1] Graduate Research Assistant, Department of Civil and Environmental Engineering, University of Illinois at Urbana-Champaign, Urbana, IL, USA, Email: msin@uiuc.edu
[2] Assistant Professor, Department of Civil and Environmental Engineering, University of Illinois at Urbana-Champaign, Urbana, IL, USA, Email: jlafave@uiuc.edu

INTRODUCTION

In reinforced concrete moment-resisting frame (RCMRF) structures under severe ground motions, beam-column connections are subjected to moment reversals across the joint due to the adjacent beams and columns. As a result, the joint regions undergo significant horizontal (and vertical) shear forces whose magnitudes are much larger than those in the adjacent members. Also, beam and column reinforcing bars passing through the joint are subjected to tension at one boundary of the joint and compression at the other because of the moment reversals. To sustain these forces, high bond stresses are required between the joint concrete and the longitudinal bars. Since both shear and bond mechanisms typically exhibit poor hysteretic properties, beam-column joints are not suitable as primary energy dissipating sources; therefore, joints are usually designed with the intention that they should remain within the elastic range of behavior.

However, it has been demonstrated by laboratory tests and post-earthquake inspections that, in ductile RCMRF structures designed based on current codes (to say nothing of older non-ductile frames), joints may in fact undergo significant inelastic shear deformations. Moreover, both elastic and inelastic shear deformations of joints may contribute greatly to story drifts in frames. Nevertheless, in seismic analyses of RCMRF structures, beam-column connections are often modeled with rigid joint zones (i.e., rigid member-end offsets in a centerline model), regardless of the joint details, while primary concern is focused on whether well-detailed beam plastic hinges can endure imposed displacement demands and whether other members can remain within their elastic ranges. Due to the "rigid joint" assumption, the contribution of joint shear deformation to overall frame displacement is neglected, and joint shear failure cannot be identified. This can result in misinterpretation of the global performance (stiffness, strength, and dynamic characteristics) of structures and could consequently lead to miscalculation of local strength and ductility demands on constituent frame members.

The primary objective of this paper is to propose a rational method for estimating the hysteretic joint shear behavior of RCMRF connections that can be incorporated into frame analysis. The focus is on ductile moment frames designed and detailed following modern seismic code requirements (rather than on older non-ductile frames with little or no joint shear reinforcement). The authors tested four RC edge beam-column-slab connection subassemblies subjected to simulated lateral loading; hysteretic joint shear behavior was investigated based on these tests and other laboratory tests reported in the literature. Then an analytical scheme employing the modified compression field theory (MCFT) was proposed to approximate joint shear stress vs. joint shear strain curves, verified based on the experimental investigations. Finally, a connection model capable of explicitly considering hysteretic joint shear behavior was formulated using DRAIN-2DX (nonlinear structural analysis software); a joint is represented by rigid elements located along the joint edges and nonlinear rotational springs embedded in one of the four hinges linking adjacent rigid elements. This connection model also takes into account fixed end rotations arising at beam/joint interfaces due to bond slip and yielding of longitudinal beam bars in the joint, as well as plastic hinge rotations at the ends of beams. Appropriate hysteretic models were adopted to represent these various nonlinear connection behaviors. The connection model was demonstrated by applying to RC beam-column connection subassemblies.

JOINT SHEAR BEHAVIOR OF RC BEAM-COLUMN CONNECTIONS

The joint shear stress vs. joint shear deformation relationship of RC beam-column connections subjected to cyclic lateral loading is characterized based on connection tests conducted by the authors, as well as other tests reported in the literature. The joint shear failure mechanism is described in terms of physical phenomena such as concrete damage and reinforcement yielding. An analytical method of estimating nonlinear hysteretic joint shear behavior is then presented.

Experimental joint shear behavior

The authors tested four cruciform RC beam-column-slab subassemblies (two concentric and two eccentric connections) subjected to quasi-static cyclic lateral loading. Each subassembly represented a 2/3-scale edge connection in an exterior moment-resisting frame, isolated at assumed inflection points between floors and between column lines. Figure 1 shows typical elevation and plan views for the specimens. The specimens were generally proportioned based on current U.S. design code requirements [1] and recommendations [2]. During testing up to a maximum of 6% story drift, all four specimens underwent some beam plastic hinging, while three of the specimens (all except one concentric connection) eventually exhibited joint shear failure. Details of the experimental program and test results can be found elsewhere [3-4].

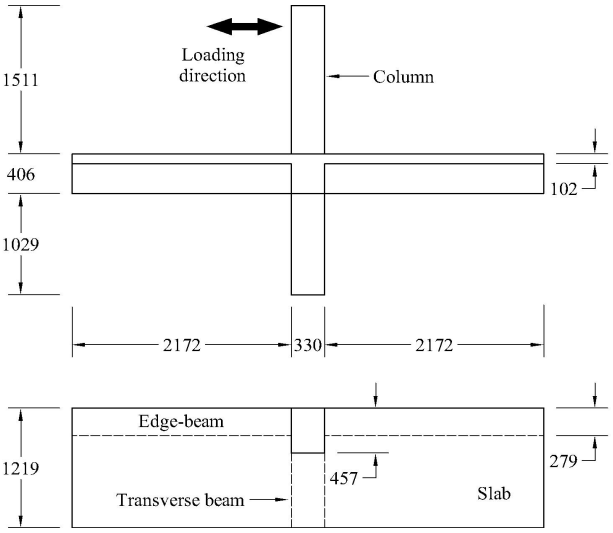

Figure 1 – Overall views of SL1 (units: mm)

The typical relationship between average joint shear stress (τ_j) and average joint shear deformation, or strain, (γ) in RCMRF structures was examined based on numerous laboratory connection tests. For example, Figure 2 shows the hysteretic $\tau_j - \gamma$ curves of specimens SL2 and SL4, obtained from the authors' tests; other tests generally showed similar patterns of cyclic joint shear behavior. Average joint shear stress was determined by dividing the horizontal joint shear force by the product of column depth and effective joint width (equal to the average of the beam and column widths). Average joint shear strain was determined using data measured by LVDTs installed extending over the entire exterior joint face.

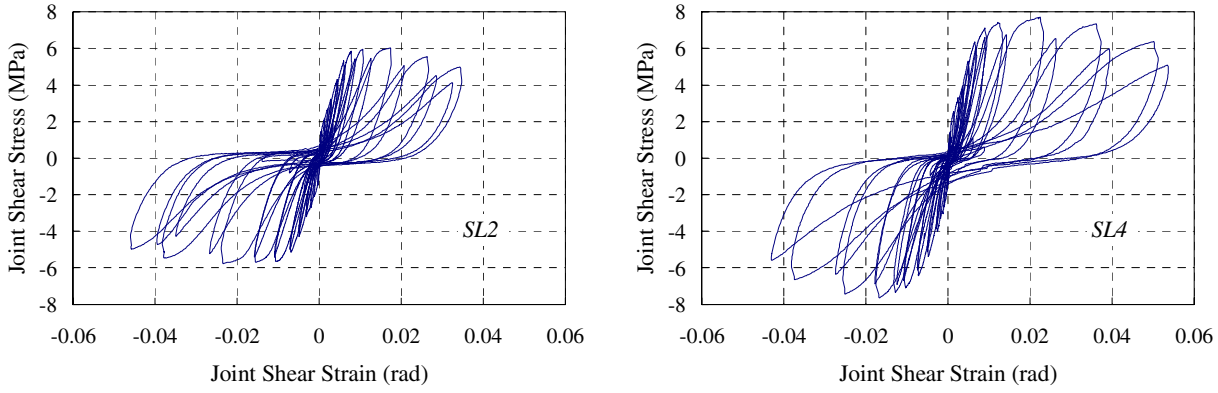

Figure 2 – Hysteretic joint shear stress vs. strain curves

Monotonic (envelope) response

Figure 3(a) plots envelope $\tau_j - \gamma$ curves for specimens SL1 through SL4 from the authors' tests, constructed by connecting the peak drift point of each cycle. Although the envelope $\tau_j - \gamma$ curves are fairly smooth, they can be simplified (for use in analysis) as four linear segments connecting three key points, so-called as *joint shear cracking* (γ_{cr}, τ_{jcr}), *reinforcement yielding* (γ_y, τ_{jy}), and *joint shear strength* (γ_m, τ_{jm}), as described in Figure 3(b). In the case of joint shear failure *after* beam hinging (as in SL1, SL2, and SL4), the second key point has been found to correspond to longitudinal beam bar yielding [4]. In the case

of joint shear failure *without* prior beam hinging, the joint reinforcement typically yields near the second key point. (Joint shear failure is defined as a condition wherein a joint cannot resist higher joint shear stress; the condition occurs at the third key point, joint shear strength.)

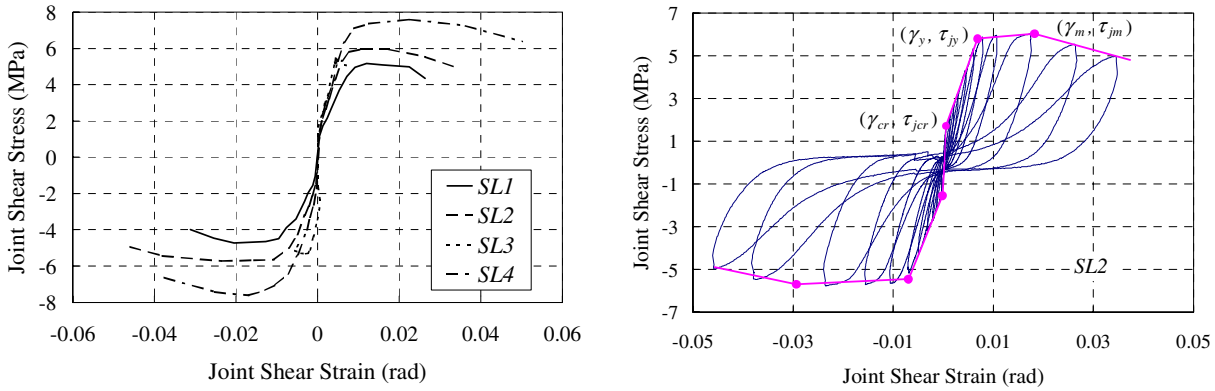

Figure 3 – (a) Envelope joint shear stress vs. strain curves; (b) simplified envelope relationship

Table 1 summarizes several connection parameters and key point ordinates of the envelope $\tau_j - \gamma$ curves determined from the authors' connection tests, and also from other tests reported in the literature that provided joint shear deformation data in addition to joint shear stress data. The authors found fifty tests that provided both joint stress and joint deformation data, but only specimens with at least half of the required joint reinforcement area per ACI 318-02 (at a spacing no greater than the limiting value) were considered in this study. All twenty-six specimens in the table were isolated cruciform (interior) connections, and a few of them included either a transverse beam and/or floor slab, as noted below the table. The specimens were tested under uni-directional quasi-static cyclic lateral loading, typically up to a maximum of 4% to 6% story drift; all of the tabulated specimens eventually failed due to joint shear, although some of them first underwent beam hinging.

Table 1 lists the joint reinforcement ratio (ρ_j) times the joint reinforcement yield strength (f_{yj}), normalized by the square root of the concrete compressive strength (f'_c); this is a comparative measure of the level of joint reinforcement among the specimens. Here, ρ_j is the joint reinforcement area in a layer divided by the vertical spacing times the column width. The table also lists the column axial load (N_c) divided by the column gross cross-sectional area (A_c), normalized by the concrete compressive strength (f'_c). With respect to reinforcement bond conditions in the joints, the column depth to beam bar diameter ratio ranged from about 11 to 30 in the specimens, with an average of 21. As for the failure mode notation, "J" stands for joint shear failure *without* beam hinging, while "BJ" indicates joint shear failure *after* beam hinging. The reported joint shear stresses were the larger of positive and negative loading values, while the joint shear strains and post-peak slopes were an average of positive and negative loading values. The key point ordinates are greatly scattered due to the different failure modes, various joint details, and the range of material properties used; there don't seem to be any clear trends in these key point ordinates with respect to the tabulated connection parameters.

The joint shear stress at shear crack initiation, τ_{jcr}, varied widely with concrete strength and column axial load, and the γ_{cr} value was typically very small (on the order of 0.0005 radians); τ_{jcr} and γ_{cr} values are not included in the table due to lack of consistent data. The γ_y values ranged from 0.002 to 0.010 radians, and γ_m was typically between 0.01 to 0.03 radians. (For most of the specimens, 0.01 radians of joint shear deformation alone would produce nearly 1% story drift.) The τ_{jy} values were approximately equal to 90% of τ_{jm} (the joint shear stress when the joint shear strength had been reached). The average of τ_{jm} values,

when normalized by the square root of the concrete compressive strength, was about 1.85√MPa in J-type failure mode specimens, while it was about 20% less in BJ-type failure mode specimens. After the point of joint shear strength (γ_m, τ_{jm}), the envelope $\tau_j - \gamma$ curves typically became flat or showed slightly descending inclination; the (negative) slope of this part (called the "post-peak slope" in Table 1) ranged from zero (horizontal) on up to about half of the average (secant) ascending slope from the origin to the point of joint shear strength; the average descending slope was about 15% of the secant ascending slope. The largest joint shear deformations reached during the tests (including behavior after the joint shear strength had been reached) were typically about 0.03 to 0.05 radians.

Table 1 – Key point ordinates for experimental joint shear stress vs. strain curves

Specimen		f'_c (MPa)	$\frac{\rho_j f_{yj}}{\sqrt{f'_c}}$ (√MPa)	$\frac{N_c}{A_c f'_c}$	Failure mode	Experimental results				
						τ_{jy} (MPa)	τ_{jm} (MPa)	γ_y (rad)	γ_m (rad)	Post-peak slope (MPa/rad)
Fujii & Morita [5]	A4	40.1	0.68	0.23	J	9.4	10.1	0.007	0.028	-52
Kurose et al.(1) [7]	J1	24.1	0.84	0.00	BJ	7.8	8.7	0.009	0.035	N.A.
Leon [8]	BCJ2	27.6	0.35	0.00	BJ	5.3	6.1	0.004	N.A.	N.A.
	BCJ3	27.6	0.35	0.00	BJ	5.5	6.8	0.003	N.A.	N.A.
Meinheit & Jirsa [9]	12	35.2	1.70	0.30	BJ	13.7	14.0	0.007	0.012	-191
	13	41.3	0.98	0.25	J	10.8	11.2	0.005	0.010	-181
	14	33.2	0.79	0.32	J	10.3	10.8	0.010	0.020	-85
Noguchi & Kashiwazaki [10]	OKJ-1	70.0	0.86	0.12	BJ	12.5	14.2	0.005	0.010	-137
	OKJ-4	70.0	0.86	0.12	BJ	12.5	15.0	0.004	0.021	0
	OKJ-5	70.0	0.86	0.12	J	13.0	14.8	0.006	0.018	-394
	OKJ-6	53.5	0.98	0.12	J	11.5	13.1	0.006	0.015	N.A.
Raffaelle & Wight [11]	1	28.6	0.68	0.02	BJ	5.2	6.0	0.004	0.014	-25
	2	26.8	0.70	0.03	BJ	4.1	4.4	0.006	0.014	-57
	3	37.7	0.59	0.02	BJ	4.0	4.9	0.005	0.017	-38
	4	19.3	0.83	0.04	BJ	3.5	4.2	0.005	0.018	-51
Shin & LaFave(2) [4]	SL1	29.9	0.48	0.00	BJ	4.9	5.3	0.009	0.016	-53
	SL2	36.2	0.44	0.00	BJ	5.8	6.2	0.007	0.021	-53
	SL4	31.2	0.96	0.00	BJ	7.1	7.7	0.008	0.020	-46
Teng & Zhou [12]	S1	33.0	0.60	0.11	BJ	8.0	8.6	0.005	0.010	-98
	S2	34.0	0.59	0.11	BJ	8.0	8.6	0.007	0.013	-119
	S3	35.0	0.58	0.10	BJ	8.0	8.3	0.010	0.022	-139
	S5	39.0	0.83	0.11	BJ	6.5	7.5	0.007	0.007	N.A.
	S6	38.0	0.84	0.11	BJ	6.5	7.3	0.007	0.015	-99
Watanabe et al. [13]	WJ-1	29.2	0.89	0.07	BJ	8.8	8.8	0.003	0.007	-138
	WJ-3	29.2	0.89	0.07	BJ	8.8	10.2	0.002	0.008	-157
	WJ-6	29.2	0.89	0.07	J	11.7	12.5	0.004	0.007	-143

Note: (1) floor slabs on both sides and (2) a floor slab and transverse beam on one side only

Some researchers [5-6] have proposed fixed values (0.005 and 0.028 radians; 0.004 and 0.01 radians, respectively) for the joint shear strains corresponding to the "reinforcement yielding" and "joint shear strength" points. However, using fixed values for the key strain points, regardless of joint details, is not reasonable in light of the above observations; therefore, a rational approach to estimate the envelope $\tau_j - \gamma$ curve of any given joint is preferred.

Hysteretic properties

As can be seen in Figure 2, cyclic $\tau_j - \gamma$ curves commonly exhibit pinching (the middle part of each hysteretic loop is relatively narrow), as well as stiffness and strength degradation (typically noted by comparing consecutive same-drift cycles). These are characteristic phenomena that also occur in plastic hinge regions of RC frame members. In joints, this behavior has been mostly attributed to shear transfer across inclined joint concrete cracks. In general, these hysteretic characteristics are negligible before joints experience initial shear cracking. Degradation of stiffness and strength greatly increases after the point of reinforcement yielding, and the extent of pinching spreads as joints are subjected to larger shear deformation cycles. The degree of each hysteretic characteristic was somewhat scattered from one specimen to another, regardless of specimen damage stages.

Description of joint shear failure mechanism

From the RC beam-column connection tests described above, it has been found that the point of reinforcement yielding corresponds to either yielding of horizontal joint reinforcement (in the case of joint shear failure *without* beam hinging) or yielding of longitudinal beam bars (in the case of joint shear failure *after* beam hinging). From this point, the envelope $\tau_j - \gamma$ curve begins to show rapid stiffness loss. In the case of joint shear failure after beam hinging, joint reinforcement yields between the points labeled as reinforcement yielding and joint shear strength. At the point of joint shear strength, a joint reaches its maximum load-carrying capacity. At about this point, joint shell concrete starts to spall off due to extensive crossing of the inclined cracks, and the joint undergoes concrete compression failure. The envelope $\tau_j - \gamma$ curve shows a negative inclination from this point onward, meaning that the joint shear strength gradually decays. Joint concrete crushing (joint shear failure) typically occurs after joint reinforcement yielding, as assumed by Bonacci and Pantazopoulou [14]. Also, Stevens et al. [15] suggested that if RC is subjected to repeat cycles of shear stress at any level above that which causes reinforcement yielding, the principal tensile strain will continue to increase with each repeat cycle, causing the concrete compressive strength to decrease until failure eventually occurs by concrete crushing.

In the case of joint shear failure *after* beam hinging, rapid stiffness loss in the envelope $\tau_j - \gamma$ curve results indirectly from beam hinging occurring near the joint, in part because the joint core starts to dilate faster after losing some confinement (that had been provided by the beams), due to large flexural cracks at beam/joint interfaces. Although the joint shear strength may be somewhat higher than the joint shear demand at the time beam hinging occurs, this strength decays under subsequent cyclic loading (of similar joint shear inputs) and can eventually become smaller than the joint shear demand imposed at beam hinging, resulting in joint shear failure [16-18]. Furthermore, the concrete strut may be required to resist a larger portion of the total joint shear (in other words, the net demand on the concrete strut may increase) when the bond condition along longitudinal beam bars deteriorates, especially after beam hinging [17].

Although RC joint shear response is somewhat influenced by connection failure mode, the joint shear stress and/or strain levels occurring in specimens that failed in a J-type mode were usually similar to (or slightly higher than) those in companion specimens that failed in a BJ-type mode. This phenomenon has been observed in many connection tests conducted on specimens designed following modern code requirements. Therefore, possible small differences in joint shear behavior between beam-column

connections that failed in the two different modes have been neglected for modeling purposes in this study.

Analytical solution for joint shear behavior

As a general solution scheme, the key point ordinates of an RC beam-column connection envelope $\tau_j - \gamma$ curve can be obtained by employing the modified compression field theory (MCFT) developed by Vecchio and Collins [19]. An RC joint core is considered as a two-dimensional (2-D) concrete panel element with uniformly distributed orthogonal reinforcement; the joint reinforcement and the longitudinal column bars are regarded as the distributed horizontal and vertical reinforcement, respectively.

In keeping with the MCFT (which considers equilibrium equations, compatibility conditions, and material constitutive laws), it is assumed that: (1) principal stress directions in the concrete coincide with principal strain directions, (2) average concrete strain in the direction of reinforcement is equal to average reinforcement strain, and (3) reinforcing steel does not resist shear (dowel action is neglected). Additionally, to simplify the analysis process, a joint core is assumed to be under uniform stress along each of the 2-D joint boundaries, as proposed for RC beams by Vecchio and Collins [20]; actual stress conditions in a joint will vary locally at each particular loading stage (because every joint boundary is actually under coupled compressive and tensile forces transmitted from the top and bottom of each beam or column). The monotonic joint shear stress (τ_j) vs. strain (γ) relationship may then be acquired for a given set of average normal (axial) stresses at the joint boundaries.

According to Collins and Mitchell [21], concrete cracking starts when the principal tensile stress in joint concrete (f_{c1}) reaches its proportional limit with respect to the principal tensile strain (ε_1):

$$f_{c1} = E_c \cdot \varepsilon_1 \left(\varepsilon_1 \le \varepsilon_{cr}\right) \text{ or } f_{c1} = \frac{\alpha_1 \cdot \alpha_2 \cdot f_{cr}}{1 + \sqrt{500\varepsilon_1}} \left(\varepsilon_1 > \varepsilon_{cr}\right)$$

Here, E_c is the modulus of elasticity of concrete (initial tangent stiffness equal to $2f'_c/\varepsilon_o$); ε_o is the strain in concrete corresponding to the concrete compressive strength (f'_c) from a standard cylinder test; f_{cr} is the concrete (tensile) cracking stress, taken as 0.5 times the square root of f'_c (in MPa); ε_{cr} is the concrete cracking strain computed by f_{cr}/E_c; and α_1 and α_2 are factors accounting for bond characteristics of the reinforcement and type of loading, respectively. As joint boundary stresses get higher, the compressive strength of joint concrete (f_{c2max}) decays with increasing principal tensile strain (ε_1) in the transverse direction:

$$f_{c2\,max} = \frac{f_c^{'}}{0.8 - 0.34\,\varepsilon_1/\varepsilon_o} \le f_c^{'}$$

The analysis stops when the principal compressive stress in concrete (f_{c2}) exceeds the reduced concrete compressive strength (f_{c2max}); in other words, the analysis cannot compute further joint shear response after the joint concrete reaches compression failure. Further details of the analysis procedures employed for acquiring the monotonic $\tau_j - \gamma$ curve of an RC joint under a given set of normal stresses can be found in the Appendix of a paper by Vecchio and Collins [19].

Figure 4 illustrates the relationship between the analytical-to-experimental maximum joint shear stress ratio and the provided-to-required joint reinforcement area ratio; each point represents one of the fifty tests found in the literature that provided both joint shear stress and deformation data [4-5,7-13,22-26]. The analytical method worked particularly well for specimens that satisfied (or at least nearly satisfied) ACI 318-02 joint reinforcement requirements. However, for specimens with relatively small areas of joint reinforcement, the analytical method gave much smaller values than the experimental results for maximum joint shear stress. This may be in part because the amount of joint reinforcement does not

actually affect joint shear strength in experimental subassemblies as much as the MCFT would predict [5,17]. The focus of this study is on ductile moment frames designed and detailed following modern seismic code requirements, a case for which the MCFT works quite well, as described in further detail below.

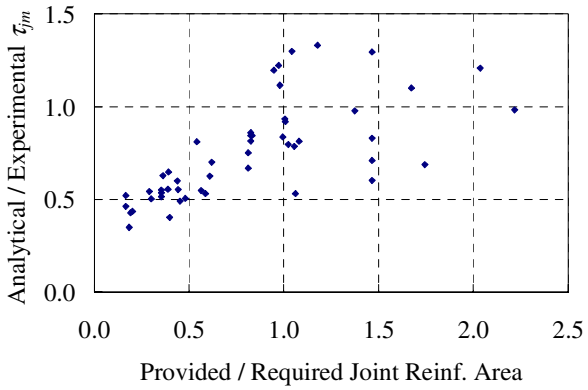

Figure 4 – Anal.-to-exp. max. joint shear stress vs. provided-to-required joint reinf. area

Figure 5 compares analytically computed envelope $\tau_j - \gamma$ curves with experimentally determined ones for two RC beam-column connections from Table 1. Specimen SL4 failed in a BJ-type mode, while specimen A4 failed in a J-type mode. Solid and dashed lines in each figure indicate (positive) experimental and analytical results, respectively, and key point ordinates for the analytical results are marked with dots. As mentioned earlier, the MCFT cannot compute further joint shear response after the joint concrete reaches compression failure. Thus, this part of the analytical joint shear stress vs. strain curve is assumed to be a straight line with a negative slope equal to 5% of the secant ascending slope up to the joint shear strength point; the descending slope is set to a somewhat smaller value than the average from the test results listed in Table 1, considering that the analytical joint shear strain at the joint shear strength point is typically a bit less than the experimental one, as explained below. The descending line forms the fourth segment of the quad-linear analytical envelope curve, as plotted in Figure 5. In the two cases, the analysis results generally match the experimental ones quite well.

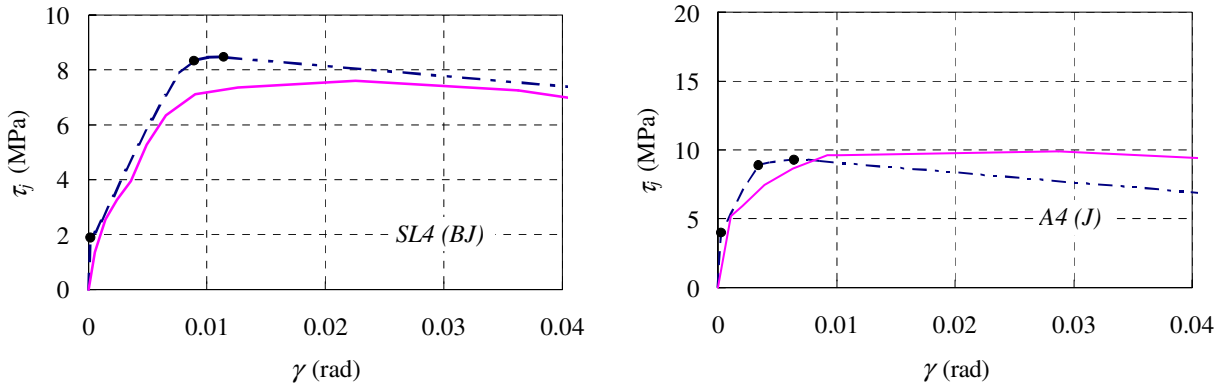

Figure 5 – Comparison between analytical and experimental envelope $\tau_j - \gamma$ curves

Analytically determined key point ordinates for the specimens in Table 1, including values for the above two specimens, are summarized in Table 2. The averages of the analytical τ_{jy} and τ_{jm} values were approximately 95% of the averages of the experimental ones, while the averages of the analytical γ_y and γ_m values were somewhat different from (about 125% and 75% of) the experimental ones. It was concluded that the proposed analytical scheme generally gave good (and slightly conservative) solutions for computing the joint shear stress vs. strain responses of RC beam-column connections with at least moderate amounts of joint reinforcement.

In combination with the analytically computed and simplified (quad-linear) envelope $\tau_j - \gamma$ curve, an appropriate hysteretic model (proposed by Foutch and Shi [27]) is adopted and calibrated to reproduce hysteretic characteristics of the experimental joint shear behavior, as presented in a later section.

Table 2 - Key point ordinates for analytical joint shear stress vs. strain curves

Specimen		Analytical results					
		τ_{jcr} (MPa)	τ_{jy} (MPa)	τ_{jm} (MPa)	γ_{cr} (rad)	γ_y (rad)	γ_m (rad)
Fujii & Morita [5]	A4	4.0	8.9	9.3	0.0003	0.003	0.006
Kurose et al.(1) [7]	J1	2.3	5.9	6.0	0.0002	0.007	0.009
Leon [8]	BCJ2	1.6	4.1	4.6	0.0002	0.004	0.011
	BCJ3	1.5	4.0	4.5	0.0002	0.004	0.011
Meinheit & Jirsa [9]	12	4.5	N.A.	13.7	0.0003	N.A.	0.005
	13	4.6	N.A.	14.9	0.0003	N.A.	0.006
	14	4.3	N.A.	12.0	0.0003	N.A.	0.006
Noguchi & Kashiwazaki [10]	OKJ-1	5.0	11.9	12.2	0.0002	0.011	0.015
	OKJ-4	5.0	11.9	12.2	0.0002	0.011	0.015
	OKJ-5	5.0	12.3	12.5	0.0002	0.011	0.014
	OKJ-6	4.1	N.A.	10.7	0.0002	N.A.	0.012
Raffaelle & Wight [11]	1	1.9	5.3	5.9	0.0002	0.006	0.011
	2	1.8	5.3	5.7	0.0002	0.006	0.010
	3	2.1	5.5	6.3	0.0002	0.005	0.012
	4	1.6	5.0	5.1	0.0002	0.006	0.008
Shin & LaFave(2) [4]	SL1	1.6	4.6	5.0	0.0002	0.007	0.014
	SL2	1.8	4.9	5.2	0.0002	0.008	0.013
	SL4	1.9	8.3	8.5	0.0002	0.009	0.011
Teng & Zhou [12]	S1	2.8	6.3	6.8	0.0002	0.004	0.008
	S2	2.8	6.4	6.8	0.0002	0.004	0.009
	S3	2.9	6.4	6.9	0.0002	0.004	0.009
	S5	2.8	8.4	9.0	0.0002	0.005	0.009
	S6	2.7	8.4	8.9	0.0002	0.005	0.008
Watanabe et al. [13]	WJ-1	2.3	6.8	7.3	0.0002	0.005	0.008
	WJ-3	2.3	6.7	7.3	0.0002	0.005	0.008
	WJ-6	2.3	7.2	7.6	0.0002	0.005	0.007

MODELING OF RC BEAM-COLUMN CONNECTION SUBASSEMBLIES

Modeling of RC beam-column connection subassemblies subjected to cyclic lateral loading is presented in this section, explicitly incorporating hysteretic joint shear behavior, as well as other appropriate inelastic behavior occurring in and around the connection. The hysteretic joint shear behavior consists of a monotonic (envelope) joint shear response analytically computed by the MCFT, and hysteretic properties calibrated based on experimental data. It is further assumed that all inelastic beam and column deformations occur in the vicinity of beam/joint or column/joint interfaces.

Element configuration in proposed model

Figure 6 illustrates a DRAIN-2DX (nonlinear structural analysis program [28]) computer model for a typical cruciform RC beam-column connection subassembly subjected to lateral loading. The joint is represented by four rigid link elements located along the joint edges and three nonlinear rotational springs embedded in one of the four hinges connecting adjacent rigid elements. DRAIN-2DX Element 10 developed by Foutch and Shi [27], which is a modified version of DRAIN-2DX Element 04 (simple connection element linking two nodes with an identical coordinate set), is used for the nonlinear rotational springs at the joint. A single Element 10 can express a bi-linear moment vs. rotation relationship as a primary curve, and it can incorporate typical hysteretic properties such as stiffness degradation, strength degradation, and pinching (see Figure 8). In this study, three such springs connected in parallel are used to represent hysteretic joint shear behavior. The hysteretic joint shear force (V_j) vs. strain (γ) curve is first determined from a hysteretic $\tau_j - \gamma$ curve described by the analytically computed and simplified (quad-linear) envelope; V_j is calculated by multiplying the joint shear stress (τ_j) by the product of column depth and effective joint width (average of the beam and column widths). Then the hysteretic moment (M_s) vs. rotation (θ_s) curve to be expressed by the combination of the three joint springs is acquired from the joint shear force (V_j) vs. strain (γ) curve by:

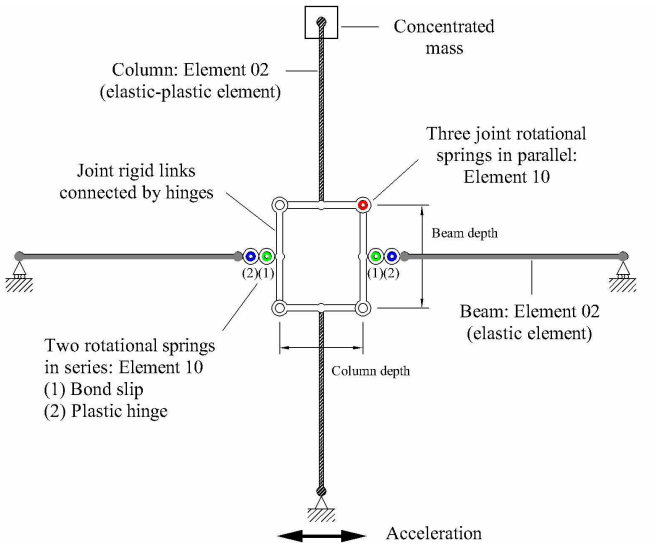

Figure 6 – DRAIN-2DX connection model

$$\theta_s = \gamma; \quad M_s = V_j \cdot jd$$

Here, *jd* is assumed to be the average of positive and negative beam moment arms at beam/joint interfaces. Figure 7 illustrates the way the three joint springs (each with a bilinear envelope) combine to express a quad-linear envelope $M_s - \theta_s$ curve. Two of the springs are elastic and then perfectly plastic, while the third spring has a negative second slope equal to that of the fourth linear segment in the quad-linear envelope $M_s - \theta_s$ curve.

Outside of the joint itself, each (upper and lower) column is modeled using one DRAIN-2DX Element 02, which consists of an elastic-perfectly plastic component and a strain-hardening (elastic) component in parallel (and Element 02 can account for axial force (P) and moment (M) interaction). Each beam is modeled using Element 02 for the elastic part and Element 10 for each of the two nonlinear rotational springs located at the beam/joint interface; the three elements are connected in series. One of the nonlinear rotational springs represents fixed end rotations arising at the beam/joint interface due to bond slip and yielding of longitudinal beam bars in the joint, while the other represents plastic hinge rotations near the end of the beam. The vertical position of the beam elements and the horizontal position of the column elements are simply located at the beam mid-depth and the column mid-depth, respectively. This beam model is similar to one proposed by Filippou et

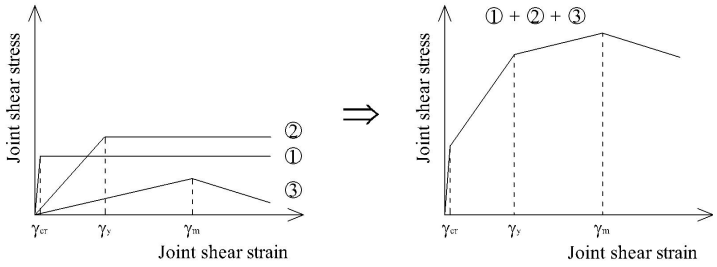

Figure 7 – Three bilinear joint springs in parallel

al. [29], which consisted of three sub-elements (elastic, spread plastic, and interface bond-slip) connected in series; however, Filippou et al. did not address hysteretic joint shear behavior, assuming that joints could be designed and detailed in order that joint shear deformations would remain small.

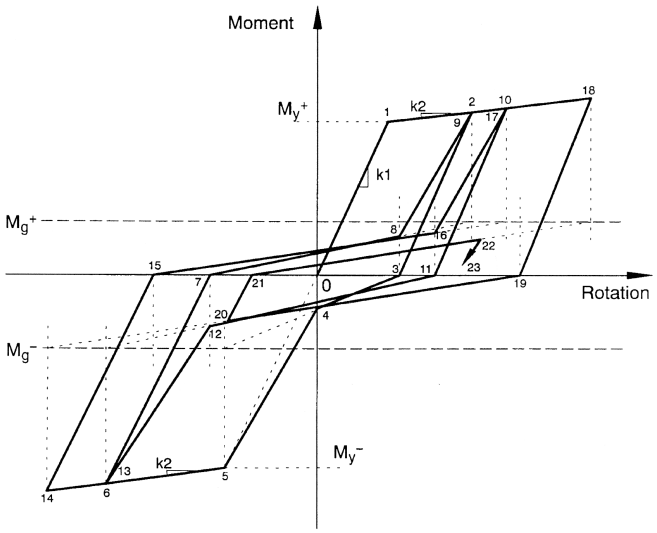

Figure 8 – Hysteretic behavior of Element 10

Details for joint modeling

The necessary input parameters for Element 10 are initial stiffness (*k1*), strain-hardening ratio (*k2/k1*), positive and negative yield moments (M_y^+ and M_y^-), strength degradation factor, and positive and negative pinching moments (M_g^+ and M_g^-), as illustrated in Figure 8. The strength degradation factor is defined as the ratio of the second to the first cycle moment at the maximum rotation reached during the first cycle, for two consecutive loading cycles (for example, the ratio between moments at the points labeled as "9" and "2" in Figure 8). The positive and negative pinching moments determine the extent of pinching in the middle part of each hysteretic loop, by designating the direction of reloading branches in conjunction with the maximum rotations reached during the previous cycle (for example, the negative pinching moment in Figure 8 specifies the slope of the line connecting the points labeled as "3" and "4"). The extent of stiffness degradation during reloading is necessarily determined from assigning pinching moments, while stiffness during unloading is kept as a constant value equal to the initial stiffness (*k1*).

All input parameters for the three joint rotational springs, except the strength degradation factors and the M_g^+ and M_g^- values, are determined from the quad-linear envelope $M_s - \theta_s$ curve, with *k2/k1* values for the first two springs set to zero. For the two elastic and perfectly plastic springs, the strength degradation factor is specified as 0.95 and the pinching moments are assumed as one-fifth of the yielding moments of each spring, while neither strength degradation nor pinching is considered for the third spring (with a negative *k2/k1* value); values for these two parameters have been approximately determined from investigating test results of the specimens listed in Table 1. The positive and negative input values for each joint spring are identical because the $\tau_j - \gamma$ curves are assumed symmetric for positive and negative loading.

Figure 9 compares the analytical and experimental joint shear response of specimen SL4; the analysis was conducted using a quasi-static displacement history simulating the peak experimental joint shear deformation of each cycle. The analytical result agrees well with the experimental one in terms of the extent of pinching and the energy dissipated in each cycle, as well as from the standpoint of envelope properties; however, the joint model could not smoothly replicate overall stiffness degradation. In general, the analytical joint model was also able to well represent the

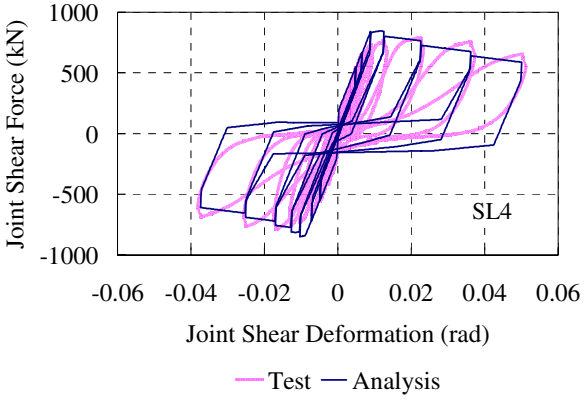

Figure 9 – Hysteretic joint shear responses from test and analysis

experimental joint shear behavior of the other beam-column connection subassemblies listed in Tables 1 and 2.

Details for beam and column modeling

The stiffness input parameters for Element 02 are the concrete elastic modulus, section moment-of-inertia, cross-sectional area, and strain-hardening ratio (ratio of post-yield slope to pre-yield slope of the moment-curvature diagram). The modulus of elasticity for concrete (E_c) was estimated from the cylinder test results by an ACI 318-02 equation.

In keeping with Paulay and Priestley [30] suggestions, the column moment-of-inertia (I_c) is taken as half the gross moment-of-inertia for columns with low axial load (when average column axial stress normalized by concrete compressive strength is less than 0.2); otherwise 70% of the gross moment-of-inertia is used. Also, the beam moment-of-inertia (I_b) is taken as 35% of the gross moment-of-inertia, computed considering the effective slab width per ACI 318-02. All of these approximate "cracked elastic" beam and column moments-of-inertia are consistent with values recommended in ACI 318-02. Gross column and beam cross-sectional areas are used. The strain-hardening ratio for the columns is computed based on yield and nominal moments and curvatures from the column moment-curvature diagram. The strain-hardening ratio for the beam elastic elements is not utilized. The column strength input parameters for Element 02 are positive and negative yield moments, compression and tension yield forces, and positive and negative balanced points of the P-M interaction curve. The beam (elastic part) strength input parameters for Element 02 are only positive and negative yield moments, which are set to very large values in order to lump all inelastic deformations at the bond slip and plastic hinge rotational springs.

For the input parameters of the moment vs. rotation relationship of the beam plastic hinge spring, the initial stiffness is assigned a large value in order to generate no rotation before yielding, and the strain-hardening ratio is set to a value equivalent to 0.03 times $6E_cI_b/l_b$ (where l_b is the full beam pin-to-pin span length minus the column depth). The yield moments are taken as the positive and negative beam yield moment strengths, computed considering the effective slab width per ACI 318-02. No strength degradation is specified, and pinching moments are assumed as one-fifth of the yielding moments, again based on experimental results.

Input parameters for the bond slip rotational spring are determined according to the formulation proposed by Morita and Kaku [31], with some modifications; assumptions and procedures used to compute the moment vs. rotation relation of the bond slip spring can be found in that paper. Modifying one Morita and Kaku suggestion, the yield moments of the bond slip spring are here taken equal to the yield moments of the plastic hinge spring in this study; the stiffness of the bond slip spring is computed with beam reinforcement only.

APPLICATION OF THE PROPOSED RC CONNECTION MODEL

The validity of the developed connection model can be demonstrated by applying it to interior RC beam-column connections listed in Tables 1 and 2. For each connection, input parameters for all elements constituting the connection model were calculated using actual material properties and member details. In the analysis process, the column axial load imposed during the test (if any) was applied first, followed by the lateral loading in a static manner.

As an example, Figure 10 compares overall story shear vs. story drift response from the analyses and the experiments for specimens SL1 and OKJ-5. During the analyses, SL1 showed joint shear failure after beam hinging, and OKJ-5 underwent joint shear failure without beam hinging, as observed in the tests. Also, the connection model characterized well the strength decay occurring after joint shear failure. The

maximum story shear force reached during the analysis of OKJ-5 was a bit smaller than the experimental one, because the analytical joint shear strength (from the MCFT) happened to be about 15% below the actual value. In both analyses, joint shear failure occurred slightly earlier than in the tests (in terms of story drift), in part because analytical joint shear strains at the point of joint shear strength were smaller than experimental ones.

In some test specimens that failed in a BJ-type mode, the developed connection model only showed either joint shear failure or beam hinging, in part because the joint and beam models (connected in series) typically have small post-yield stiffness. For instance, the joint shear response obtained from the analysis of specimen SL4 never got to the point of joint shear failure (up to 6% story drift), as the analytical joint shear strength was somewhat larger than the experimental joint shear stresses. However, even in this case analytical joint shear deformations contributed more than 20% to the overall story drift of the connection model, a feature that would have been lost without considering joint shear deformations in the model. In conclusion, the developed connection model was able to well represent the overall experimental load-displacement response of connection subassemblies, and it is therefore likely well-suited for use in RC frame analyses.

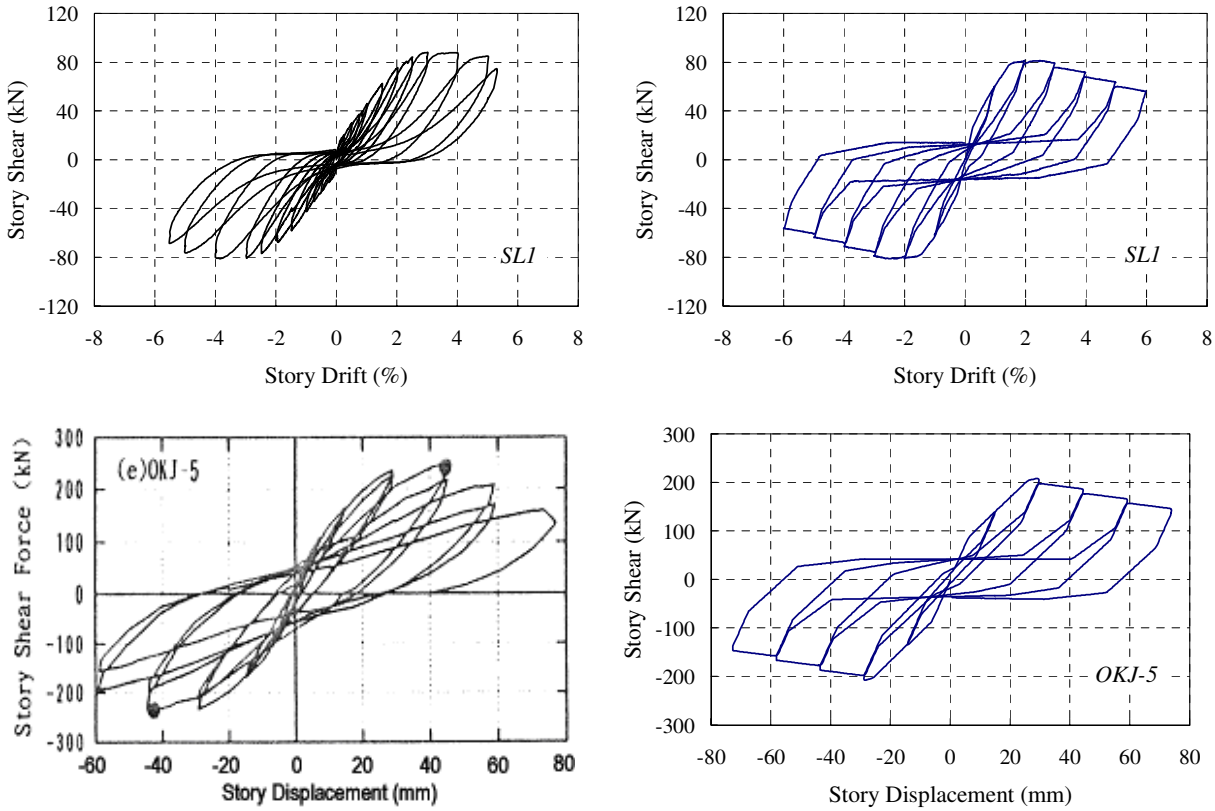

Figure 10 – Comparison of overall load-displacement responses from tests and analyses

CONCLUSIONS

This study proposes an analytical method for estimating the hysteretic joint shear behavior of RC beam-column connections and develops a DRAIN-2DX connection model capable of explicitly incorporating this behavior into frame analysis. A summary of key findings and conclusions is as follows:

- From investigating numerous beam-column connection tests, nonlinear hysteretic joint shear stress vs. strain behavior was characterized as a quad-linear envelope curve (connecting the points

of joint shear cracking, reinforcement yielding, and joint shear strength) with a descending slope after failure and typical RC hysteretic properties.

- An analytical scheme was utilized to estimate the nonlinear hysteretic shear stress vs. strain response of beam-column joints without testing. The envelope curve of joint shear response was computed using the MCFT, while the hysteretic properties were represented by an appropriate hysteresis model, calibrated based on experimental results. In general, the proposed analytical scheme gave good results in comparison with experiments.
- A connection model was developed to explicitly incorporate nonlinear joint shear behavior into frame analysis. (The connection model also addressed fixed end rotations at beam/joint interfaces due to bond slip and yielding of longitudinal beam bars in the joint, as well as plastic hinge rotations near the ends of beams.) The connection model was able to well represent the overall cyclic load-displacement response of beam-column connection subassemblies, and to capture contributions from the beams, the columns, and the joint to overall story drift.
- The developed connection model, along with the proposed analytical scheme for joint shear response, can further be used to evaluate global performance of RC frame structures, including estimates of local strength and ductility demands on constituent frame members. This connection model can be particularly effective in the analysis of frame structures where moderate to large joint shear deformations may occur.

REFERENCES

1. ACI Committee 318. *Building code requirements for reinforced concrete (ACI 318-02) and commentary (ACI 318R-02)*, American Concrete Institute, Farmington Hills, Michigan, 2002.
2. ACI-ASCE Committee 352. *Recommendations for design of beam-column connections in monolithic reinforced concrete structures (ACI 352R-02)*, American Concrete Institute, Farmington Hills, Michigan, 2002.
3. Shin M, LaFave JM. "Seismic performance of reinforced concrete eccentric beam-column connections with floor slabs," *ACI Structural Journal*, 2004, 101, in press.
4. Shin M, LaFave JM. "Reinforced concrete edge beam-column-slab connections subjected to earthquake loading," *Magazine of Concrete Research*, 2004, 56, in press.
5. Fujii S, Morita H. "Comparison between interior and exterior RC beam-column joint behavior," *Design of Beam-Column Joints for Seismic Resistance (SP-123)*, American Concrete Institute, Detroit, Michigan, 1991, 145-165.
6. Teraoka M, Fujii S. "Seismic damage and performance evaluation of R/C beam-column joints," *The Second US-Japan Workshop on Performance-Based Engineering for Reinforced Concrete Building Structures*, Hokkaido, Japan, 2000, 379-390.
7. Kurose Y, Guimaraes GN, Zuhua L, Kreger ME, Jirsa JO. "Evaluation of slab-beam-column connections subjected to bi-directional loading," *Design of Beam-Column Joints for Seismic Resistance (SP-123)*, American Concrete Institute, Detroit, Michigan, 1991, 39-67.
8. Leon RT. "Shear strength and hysteretic behavior of interior beam-column joints," *ACI Structural Journal*, 1990, 87(1), 3-11.
9. Meinheit DF, Jirsa JO. "Shear strength of RC beam-column connections," *Journal of the Structural Division*, ASCE, 1981, 107(ST11), 2227-2244.
10. Noguchi H, Kashiwazaki T. "Experimental studies on shear performances of RC interior column-beam joints with high-strength materials," *Tenth World Conference on Earthquake Engineering*, Balkema, Rotterdam, 1992, 3163-3168.
11. Raffaelle GS, Wight JK. "Reinforced concrete eccentric beam-column connections subjected to earthquake-type loading," *ACI Structural Journal*, 1995, 92(1), 45-55.

12. Teng S, Zhou H. "Eccentric reinforced concrete beam-column joints subjected to cyclic loading," *ACI Structural Journal*, 2003, 100(2), 139-148.
13. Watanabe K, Abe K, Murakawa J, Noguchi H. "Strength and deformation of reinforced concrete interior beam-column joints," *Transactions of the Japan Concrete Institute*, 1988, 10, 183-188.
14. Bonacci J, Pantazopoulou S. "Parametric investigation of joint mechanics," *ACI Structural Journal*, 1993, 90(1), 61-71.
15. Stevens NJ, Uzumeri SM, Collins MP. "Reinforced concrete subjected to reversed cyclic shear – experiments and constitutive model," *ACI Structural Journal*, 1991, 88(2), 135-146.
16. Joh O, Goto Y, Shibata T. "Behavior of reinforced concrete beam-column joints with eccentricity," *Design of Beam-Column Joints for Seismic Resistance (SP-123)*, American Concrete Institute, Detroit, Michigan, 1991, 317-357.
17. Kitayama K, Otani S, Aoyama H. "Development of design criteria for RC interior beam-column joints," *Design of Beam-Column Joints for Seismic Resistance (SP-123)*, American Concrete Institute, Detroit, Michigan, 1991, 97-123.
18. Kitayama K. "Restoring force characteristics in reinforced concrete beam-column joints," *Transactions of the Japan Concrete Institute*, 1992, 14, 491-498.
19. Vecchio FJ, Collins MP. "The modified compression field theory for reinforced concrete elements subjected to shear," *ACI Structural Journal*, 1986, 83(2), 219-231.
20. Vecchio FJ, Collins MP. "Predicting the response of reinforced concrete beams subjected to shear using modified compression field theory," *ACI Structural Journal*, 1988, 85(3), 258-268.
21. Collins MP, Mitchell D. *Prestressed Concrete Structures*, Prentice Hall, Upper Saddle River, NJ, 1991.
22. Endoh Y, Kamura T, Otani S, Aoyama H. "Behavior of R/C beam-column connections using light-weight concrete," *Transactions of the Japan Concrete Institute*, 1991, 13, 319-326.
23. Kitayama K, Asakura H, Otani S, Aoyama H. "Earthquake resistant design criteria for reinforced concrete interior beam-column joints," *Transactions of the Japan Concrete Institute*, 1988, 10, 281-288.
24. Kitayama K, Lee S, Otani S, Aoyama H. "Behavior of high-strength R/C beam-column joints," *Tenth World Conference on Earthquake Engineering*, Balkema, Rotterdam, 1992, 3151-3156.
25. Morita S, Kitayama K, Koyama A, Hosono T. "Effects of beam bar bond and column axial load on shear strength in reinforced concrete interior beam-column joints," *Transactions of the Japan Concrete Institute*, 1999, 21, 453-460.
26. Owada Y. "Three-dimensional behaviors of reinforced concrete beam-column joint under seismic load," *Twelfth World Conference on Earthquake Engineering*, Auckland, New Zealand, 2000, Paper no. 0707.
27. Foutch DA, Shi S. *Connection element (type 10) for DRAIN-2DX*, Internal Report, University of Illinois, Urbana, Illinois, 1997.
28. Prakash V, Powell GH, Campbell S. *DRAIN-2DX base program description and user guide*, University of California, Berkeley, California, 1993.
29. Filippou FC, D'Ambrisi A, Issa A. "Effects of reinforcement slip on hysteretic behavior of reinforced concrete frame members," *ACI Structural Journal*, 1999, 96(3), 327-335.
30. Paulay T, Priestley MJN. *Seismic Design of Reinforced Concrete and Masonry Buildings*, John Wiley & Sons, New York, NY, 1992.
31. Morita S, Kaku T. "Slippage of reinforcement in beam-column joint of reinforced concrete frame," *Eighth World Conference on Earthquake Engineering*, San Francisco, CA, 1984, 477-484.